



**HAL**  
open science

# Synergetic Effect of Discontinuous Carbon Fibers and Graphite Flakes on Thermo-Mechanical Properties of Aluminum Matrix Composites Fabricated by Solid–Liquid Phase Sintering

Nabil Chamroune, Florence Delange, Nathalie Caillault, Fabrice Morvan,  
Yongfeng Lu, Akira Kawasaki, Jean-François Silvain

► **To cite this version:**

Nabil Chamroune, Florence Delange, Nathalie Caillault, Fabrice Morvan, Yongfeng Lu, et al.. Synergetic Effect of Discontinuous Carbon Fibers and Graphite Flakes on Thermo-Mechanical Properties of Aluminum Matrix Composites Fabricated by Solid–Liquid Phase Sintering. *Metals and Materials International*, 2020, 26 (2), pp.155-167. 10.1007/s12540-019-00324-0 . hal-02294346

**HAL Id: hal-02294346**

**<https://hal.science/hal-02294346>**

Submitted on 16 Jul 2020

**HAL** is a multi-disciplinary open access archive for the deposit and dissemination of scientific research documents, whether they are published or not. The documents may come from teaching and research institutions in France or abroad, or from public or private research centers.

L'archive ouverte pluridisciplinaire **HAL**, est destinée au dépôt et à la diffusion de documents scientifiques de niveau recherche, publiés ou non, émanant des établissements d'enseignement et de recherche français ou étrangers, des laboratoires publics ou privés.

1 Synergetic effect of discontinuous carbon fibers and graphite flakes on thermo-mechanical  
2 properties of aluminum matrix composites fabricated by solid-liquid phase sintering

3

4 Nabil Chamroune<sup>1</sup>, Florence Delange<sup>2</sup>, Nathalie Caillault<sup>2</sup>, Fabrice Morvan<sup>3</sup>, Yongfeng Lu<sup>4</sup>, Akira Kawasaki<sup>5</sup>,  
5 Jean-François Silvain<sup>1, 4\*</sup>

6

7 <sup>1</sup>CNRS, Univ. Bordeaux, Bordeaux INP, ICMCB, UMR 5026, F-33600 Pessac, France

8 <sup>2</sup>Schneider Electric SAS, 38TEC, Rue Henry Tarze, 38000 Grenoble, France

9 <sup>3</sup>Toyol Europe SASU, Rte de Lescun, 64490 Accous, France.

10 <sup>4</sup>Department of Electrical and Computer Engineering, University of Nebraska-Lincoln, Lincoln, NE, 68588-0511,  
11 USA

12 <sup>5</sup>Department of Materials Processing, Graduate School of Engineering, Tohoku University, 6-6-02 Aramaki-aza  
13 Aoba, Aoba-ku, Sendai, Miyagi 980-8579, Japan

14

15 \*Corresponding author:

16 Dr. Jean-Francois Silvain, ICMCB-CNRS, 87 Avenue du Dr Albert Schweitzer, F-33608 Pessac cedex, France.

17 Phone : +33 (0)5 40 00 84 37

18 Email address: jean-francois.silvain@icmcb.cnrs.fr

19

20

21 Abstract

22 Aluminum (Al) matrix composite materials reinforced with graphite flakes (GF) and pitch-based carbon fibers  
23 (CF) were fabricated by solid-liquid phase sintering with a small amount of Aluminum-Silicon eutectic alloy (Al-  
24 12wt%Si). The amount of Al-Si is optimized for a carbon content of 50 vol.% in order to achieve, in the plane of  
25 GF reinforcement, a higher thermal conductivity (TC) and a lower coefficient of thermal expansion (CTE)  
26 compared to identical composite material fabricated by conventional powder metallurgy route. Al/(GF+CF)  
27 composite materials were characterized by scanning electron microscopy (SEM), energy-dispersive X-ray  
28 microscopy and X-ray tomography in order to highlight the distribution of the Al-Si liquid phase and the formation

29 of a carbon network in the aluminum matrix. A small amount of CF allows to control the through-plane CTE  
30 without affecting significantly the in-plane TC of the Al-C composites. The (GF+CF) mixture and the solid-liquid  
31 phase sintering allow to achieve a TC of 410 W/m.K (in-plane direction) and a CTE of  $2.4 \times 10^{-6}$  /K (through-plane  
32 direction), which is, for example, applicable for lightweight heat sink material.

33 Keywords

34 Metal-matrix composites (MMCs); Discontinuous reinforcement; Powder processing; Thermal properties

35

36 1. Introduction

37 Metal matrix composite materials (MMC) are currently studied and have several promising applications. One of  
38 them concerns their use as heat sinks in microelectronic industries where two conditions are required: a thermal  
39 conductivity (TC) as high as possible in order to evacuate the heat generated by the silicon chip and therefore to  
40 increase the reliability of the electronic device, and a coefficient of thermal expansion (CTE) close to the CTE of  
41 ceramic substrate ( $2$  to  $8 \times 10^{-6}$  /K) and the electronic chip ( $2$  to  $4 \times 10^{-6}$  /K) [1-4]. Currently Copper (Cu) and  
42 Aluminum (Al) heat sinks are used because of their high TC ( $400$  W/mK for Cu and  $220$  W/mK for Al). However,  
43 the large CTE mismatch with the ceramic substrate (CTE of Cu equal to  $17 \times 10^{-6}$  /K and CTE of Al equal to  $24 \times 10^{-6}$   
44 /K) generates thermo-mechanical stresses at the heat sink-ceramic interfaces which can generate cracks inside  
45 the solder joint of inside the ceramic substrate and then catastrophic failure of the electronic device.

46 Compared to the others matrices (Copper or Silver), Aluminum has a lower TC and a higher CTE. However, due  
47 to his low density,  $2.7 \text{ g/cm}^3$ , and low price, Al has a high specific thermal conductivity (TC divided by density)  
48 and low cost which is a great advantage in terms of the fabrication of mobile electronic devices for automobile or  
49 aeronautic industries [4].

50 Among carbon reinforcements, diamonds exhibit outstanding isotropic thermal properties (TC of  $\sim 2000$  W/m.K  
51 and CTE close to  $2.5 \times 10^{-6}$  /K) [5-7]. However, the applications are limited due to its high price and poor  
52 machinability. Pitch-based carbon fibers (FC) are in contrast less expensive and have a good machinability but a  
53 lower and anisotropic thermal properties (longitudinal direction: TC of  $100$ - $1000$  W/m.K depending on  
54 graphitization degree and CTE of  $-1 \times 10^{-6}$  /K ; transverse direction: TC of  $5$ - $10$  W/m.K and CTE of  $12 \times 10^{-6}$  /K) [8,  
55 9]. Graphite flakes (GF) have significant attention for thermal management applications due to their superior  
56 thermal properties, low cost and ease of machining. Indeed it has been reported that GF exhibit a CTE of  $-1 \times 10^{-6}$   
57 /K and a TC higher than  $1000$  W/m.K in the plane of graphite flake [10, 11]. A TC of  $1600$ - $2000$  W/m.K has been  
58 reported for highly oriented pyrolytic graphite (HOPG) [12, 13]. Out of plane, whatever the graphite type, a TC of  
59  $5$ - $10$  W/m.K and a CTE of  $28 \times 10^{-6}$  /K has been reported [11, 13, 14].

60 In functional metal matrix composite (MMC), extended works have been reported on reactivity between matrix  
61 and reinforcement [15, 16], dispersion and orientation of reinforcement [17, 18], fabrication process [4] (sintering  
62 [10, 18], squeeze casting [10, 20] and pressure infiltration process [21]). However, few attempts in solid-liquid  
63 phase sintering [22] have been carried out especially with a mixture of GF and CF reinforcements. Pietro et al.  
64 [23] and Oddone et al. [24] reported composites with a mixture of GF and CF, fabricated by gas pressure infiltration  
65 and spark plasma sintering, respectively. They focused their studies on sintering parameters (heating rate, current

66 flow and sintering temperature) and the nature of the metal. However, no understanding on the behavior of the  
67 thermal properties of Metal/(GF+CF) compared to the Metal/GF and Metal/CF composite materials was reported.  
68 Several studies reported the fabrication of metal/GF composite materials with a significant increase of TC along  
69 the GF principal axis (in-plane TC) and a decrease of TC perpendicular to the GF principal axis (through-plane  
70 TC) [25, 26]. However, concerning the CTE of MMC, studies reported a slight decrease of the in-plane CTE and,  
71 surprisingly, a significant decrease of through-plane CTE [26, 27, 28, 29]. In Cu/50vol.%GF systems, through-  
72 plane CTE of  $2.5 \times 10^{-6}$  /K [26],  $1.9 \times 10^{-6}$  /K [27] and  $-1 \times 10^{-6}$  /K [28] was reported, which is very close to CTE of  
73 silicon ( $2.8 \times 10^{-6}$  /K). In Al/50vol.%GF systems, a through-plane CTE of  $-10 \times 10^{-6}$  /K and an in-plane TC of 330  
74 W/m.K were reported [29]. However, this CTE presents a significant CTE mismatch with the ceramic substrate.  
75 Therefore, in order to obtain a CTE close to  $3 \times 10^{-6}$  /K in Al/GF system, the vol.% of GF must be decreased which  
76 will, consequently, decreases the TC of Al/GF composite [29].

77 This investigation reports a way to control the CTE of Al/C composite by adding small quantity of CF to Al/GF  
78 composites in order to obtain a CTE compatible to the ceramic in the in-plane or the through-plane direction.  
79 Al/Carbon composites materials were fabricated by solid-liquid phase sintering. The quantity of Al-12wt%Si alloy,  
80 in liquid state during the sintering process, was optimized for a total carbon content of 50 vol.% in order to obtain  
81 fully dense (Al+Al-Si)/Carbon materials. Different GF/CF ratios was used in order to investigate the effect of the  
82 solid-liquid phase sintering and the carbon composition on the TC and the CTE of the (Al+Al-Si)/(GF+CF)  
83 composite materials. Al/C composite materials were characterized by scanning electron microscopy (SEM),  
84 energy-dispersive X-ray microscopy (EDS) and X-ray tomography in order to understand the behavior of thermo-  
85 mechanical properties of Al/(GF+CF) composite materials.

86

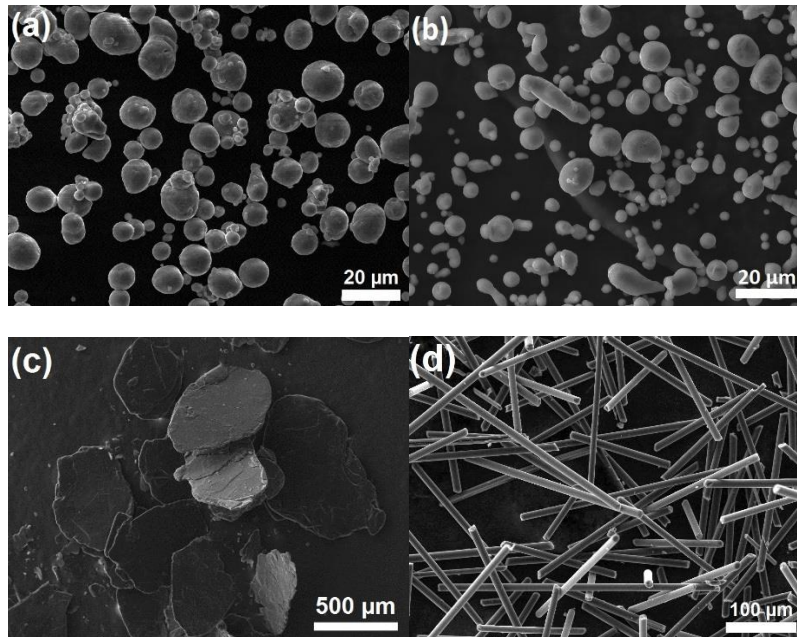
## 87 2. Experimental procedure

### 88 2.1. Materials

89 Gas-atomized Al spherical powder (ULTD0065, Hermillon powders, France, Fig. 1a) and Al-12wt%Si spherical  
90 powder (16-0006G, Toyal, Japan, Fig. 1b) with an average diameter of 10  $\mu$ m and 8  $\mu$ m, respectively, were used  
91 as the starting metal powder. Graphite Flakes (GF; Yanxin-Graphite Co., Ltd, Fig. 1c), with an average size and  
92 thickness of 550  $\mu$ m and 30  $\mu$ m respectively, and Carbon Fibers (CF, K223HM, CTN DIALEAD™/BOBBINS,  
93 Sumitomo Corporation Europe Limited, Fig. 1d) with an average length and diameter of 250  $\mu$ m and 10  $\mu$ m

94 respectively, were added to metal powder. The four components were mixed in Turbula mixer (Turbula  
95 Shaker/Mixer Model T2C, Germany) for 2 hours to obtain a homogeneous (Al+AlSi)/(GF+FC) distribution.

96

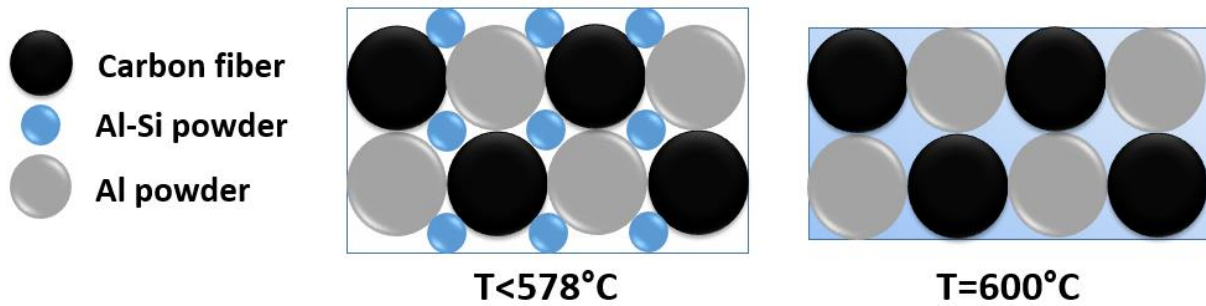


97

98 **Figure 1:** SEM micrographs of starting materials: (a) Al powder, (b) Al-Si powder, (c) Graphite flakes (d) Carbon  
99 fibers

100

101 After compacting the (Al+Al-Si)/C mixture in a steel mold, cylindrical bulk (Al+Al-Si)/C composites ( $\text{Ø}10 \times 8$   
102  $\text{mm}^3$ ) were fabricated by hot pressing for 30 min at  $600^\circ\text{C}$  under a uniaxial compressive stress of 60 MPa and  
103 primary vacuum. The temperature of the steel mold is measure with a thermocouple place inside the mold and  
104 close to the composite powder. Heating time is close to 10 min and cooling time to 60 min. Differential thermal  
105 analysis of Al-Si alloy powder has shown that the melting temperature is  $578^\circ\text{C}$ . For these processing conditions,  
106 Al-Si alloy is in liquid state during the densification of the materials as illustrated in Figure 2. The volume fraction  
107 of GF and CF in the Al/GF and Al/CF composites respectively, was fixed at 10, 20, 30, 40, and 50%. Concerning  
108 Al/(GF+CF) composite materials, the composition of the carbon mixture (vol.%GF + vol.%CF) was fixed at  
109 (48+2), (46+4), (44+6), (42+8), (40+10), (30+20), (20+30) and (10+40) for a total carbon volume fraction of 50  
110 vol.%. The hot-pressing temperature was monitored via a K-type thermocouple located 2 mm from the sample in  
111 the steel mold. Considering that the GF and carbon fibers [8, 18] tend to be aligned perpendicularly to the uniaxial  
112 compressive stress, the cylindrical Al/GF composites were machined to  $\text{Ø}6 \times 5 \text{ mm}^3$  in order to measure TC and  
113 CTE in the in-plane and through-plane direction.



114

115 Figure 2: Illustration of the solid-liquid phase sintering process. The initial powder mixture (Al+Al-Si+C) is  
 116 sintered under 60 MPa at 600°C which result in the fusion of the Al-12wt%Si alloy.

117

118 2.2. Characterization

119 Microstructural characterization of the Al/GF composite was carried out via scanning electron microscopy (SEM,  
 120 Tescan, VEGA© II SBH). Elemental analysis of the Al/C composites was performed through energy dispersive  
 121 X-ray spectroscopy (EDS, Apollo X, EDAX Inc.). In order to reveal the microstructure, Al/GF composites were  
 122 prepared using mechanical polishing with polishing cloth. The polished samples were placed in etchant aqueous  
 123 solution of sodium hydroxide.

124 X-Ray tomography was carried out via micro-scanner (General Electrics V/Tome/x s). The acquisition resolution  
 125 is equal to 2.8  $\mu\text{m}^3$ . The voltage and rotation resolution are equal to 180 kV and 0.1°, respectively. The dimension  
 126 of the sample is  $\text{Ø}6 \times 5 \text{ mm}^3$  and  $2.5 \times 2.5 \times 5 \text{ mm}^3$ . Tomography data were treated with ImageJ software.

127 The CTE of the Al/C composite materials was measured with a dilatometer (NETZSCH DIL 402, PC) in two  
 128 thermal cycles from 40°C to 300°C with a heating/cooling rates of 2°C/min, under argon gas flow. The technical  
 129 mean values of CTE were recorded between 50°C and 150°C. Each measure point is an average of 3 samples with  
 130 a standard deviation close to 3%.

131 Heat capacity was measured by differential Scanning Calorimetry at 70°C (DSC 8000 Pyris Diamond PERKIN  
 132 ELMER) for graphite flake, carbon fiber, Al-Si and Al powders. The TC of Al/GF composites was calculated  
 133 using the following equation  $\text{TC} = \alpha \times \rho \times C_p$  where  $\alpha$  is the thermal diffusivity of Al/GF composites measured via  
 134 the laser flash method (NETZSCH LFA 45, MicroFlash) at 70°C. Each measure point is an average of 3 samples  
 135 with a standard deviation close to 5%. The thermal diffusivity was measured in the in-plane and transverse  
 136 direction.  $C_p$  and  $\rho$  are the heat capacity and the measured density of the Al/GF composites, respectively.  $C_p$  was  
 137 calculated from heat capacity of each component by a rule of mixture. Considering that the composite materials

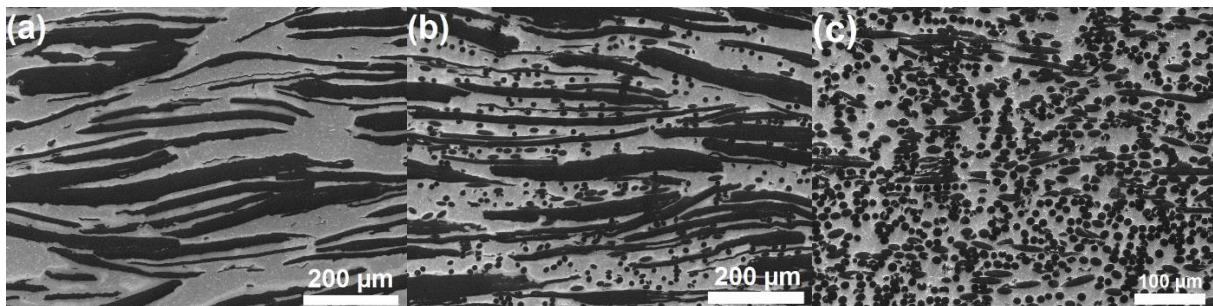
138 only contain closed porosity (ranging from 0.2 to 2.5%), the density of the Al/C composites was measured using  
139 the Archimedes principle. The theoretical density of the composites was calculated using a rule of mixture.

140

### 141 3. Results and discussion

#### 142 3.1. Microstructure analysis

143 Figure 3 shows the in-plane view SEM micrographs of the Al/50vol.%GF (Fig. 3a), Al/vol.%(40GF+10CF) (Fig.  
144 3b), and Al/50vol.%CF (Fig. 3c) composite materials. Dark contrasts are associated to graphite flake (black  
145 rectangle) and carbon fiber (black circle) and gray one refers to Al matrix. At that scale of resolution, identical  
146 microstructure are found for the Al(Al-Si) matrix. For Al/50vol.%GF and Al/vol.%(40GF+10CF) composites,  
147 graphite flakes are preferentially oriented in a plane perpendicular to the pressure direction. In the case of  
148 Al/50vol.%(GF+CF), the presence of CF does not affect the orientation of GF compared to Al/GF composite  
149 materials. In Al/50vol%CF composites, carbon fibers are also oriented in the plane perpendicular to the pressure  
150 direction but randomly oriented in this plan. Moreover, because of the high-volume fraction of carbon  
151 reinforcement (50 vol.%), GF-GF (Fig. 4a), GF-CF (Fig. 3b) and CF-CF (Fig. 3c) contact points are observed in  
152 all of the Al/C composites materials.



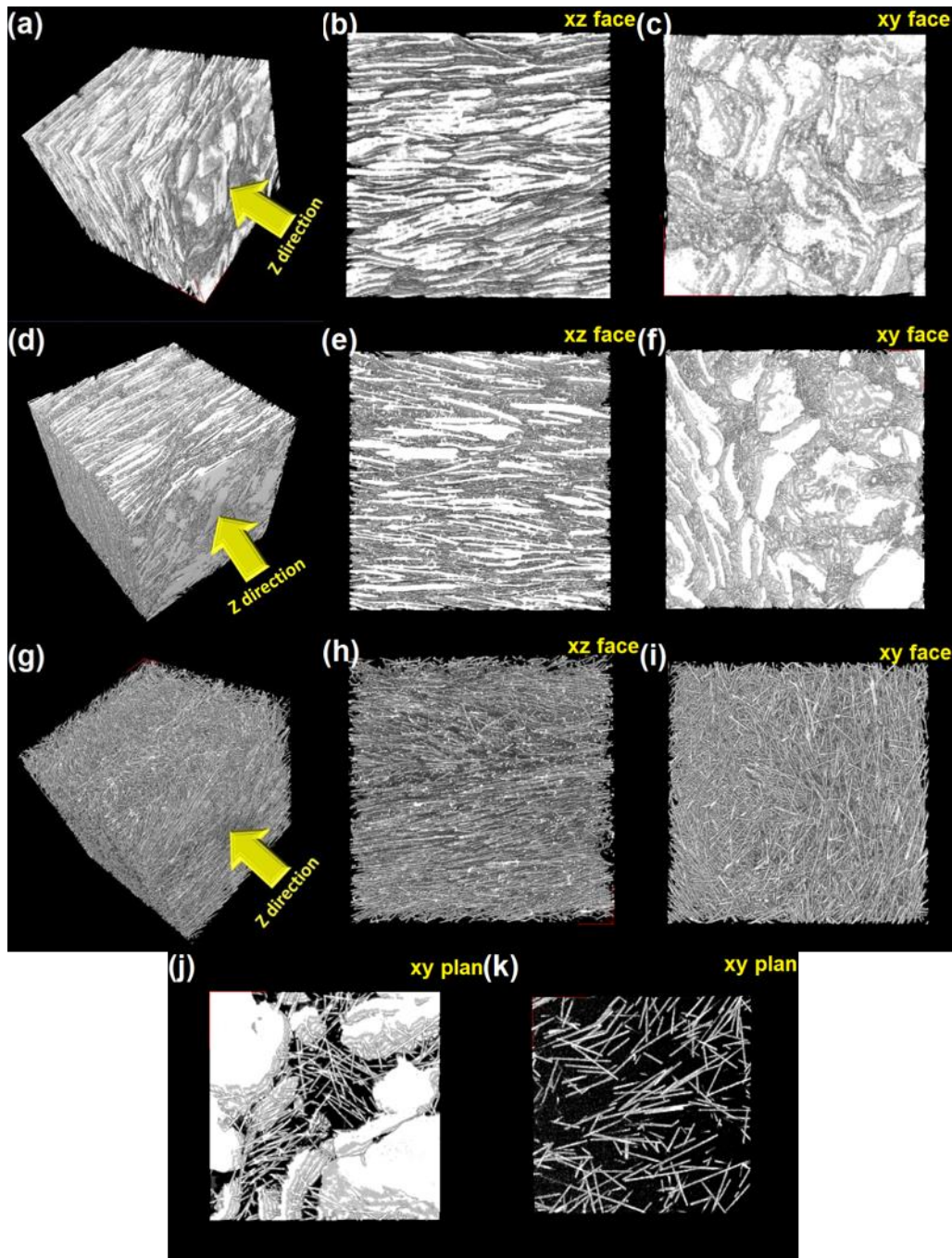
153

154 Figure 3: SEM micrographs (in-plane view) of (a) Al/50vol%GF, (b) Al/(40vol.%GF+10vol.%CF) and (c)  
155 Al/50vol%CF composite materials

156

157 Figure 4 shows X-Ray tomography analysis of Al/50vol.%GF (a, b, and c), Al/vol.%(40GF+10CF) (d, e, f and j)  
158 and Al/50vol.%CF (g, h, i, and k) composite materials. The carbon network of Al/50vol.%GF,  
159 Al/vol.%(40GF+10CF) and Al/50vol.%CF composites were reconstructed in a cubic block of 1.84 mm<sup>3</sup>. Yellow  
160 arrows show the pressure direction (Z axis) applied during the sintering process. These reconstructions clearly  
161 show different microstructure observed in (xz) and (xy) plan which is characteristic of a transversally isotropic

162 material. In the (xy) plan, the top surface of the GF can be observed (Fig. 4c, 4f and 4j) whereas the CF are  
163 randomly oriented (Fig. 4f, 4i and 4k). In the (xz) plan, the section of GF and CF can be observed.



164

165

166 Figure 4: X-Ray tomography analysis of: (a), (b), and (c) Al/50vol.%GF; (d), (e), (f,) and (j) and  
167 Al/(40vol.%GF+10vol.%CF); (g), (h,) (i) and (k) Al/50vol.%CF composite materials. (Yellow arrows show the  
168 pressure direction)

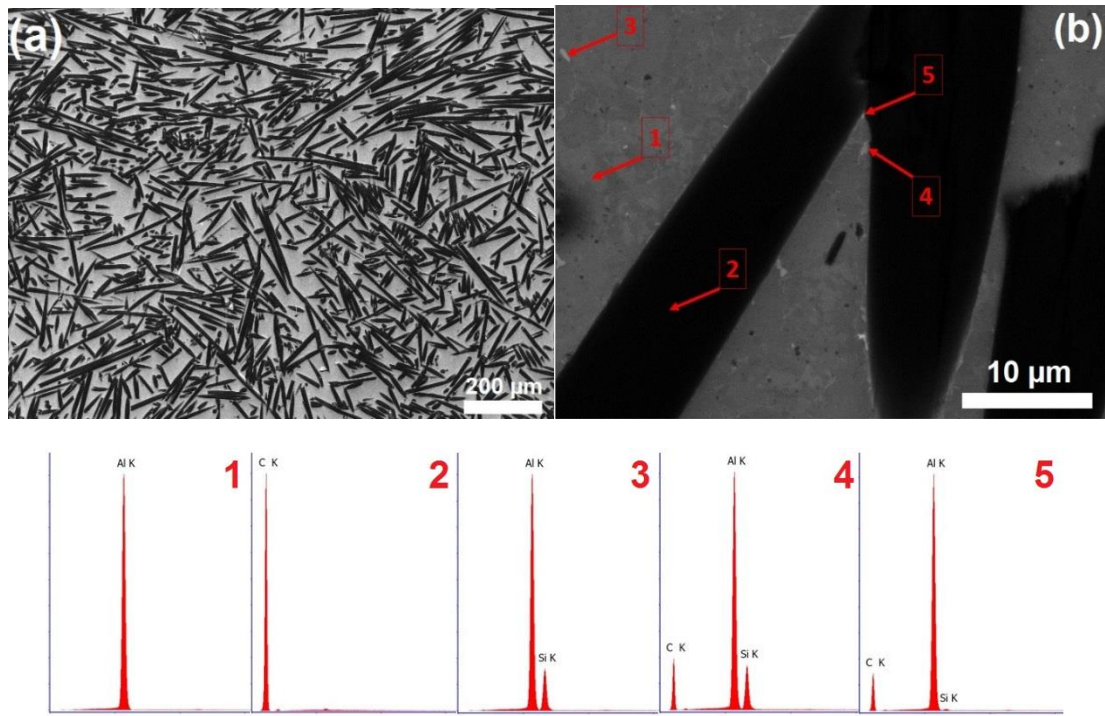
169

170 These observations imply that the pressure applied during the hot pressing provides an orientation of the carbon  
171 reinforcement perpendicular to the pressure axis. It has to be noticed that in some area, carbon reinforcement is  
172 still disoriented [18]. Moreover, the carbon network of Al/vol.%(40GF+10CF), Al/50vol.%CF were reconstructed  
173 in a square of  $1.1 \times 1.1 \text{ mm}^2$  and a thickness of  $30 \text{ }\mu\text{m}$  (Fig. 4j and 4k).

174 This allows highlighting the formation of a continuous 2D carbon networks composed by GF and CF oriented  
175 randomly in this same plan. However, by comparing Al/vol.%(40GF+10CF) and Al/50vol.%CF, which have the  
176 same carbon content, it can be seen an as dense carbon fiber network in Al/vol.%(40GF+10CF) than  
177 Al/50vol.%CF. Indeed, in Al/50vol.%CF, the carbon fibers are dispersed in 50 vol.% of Al whiles in  
178 Al/vol.%(40GF+10CF), the CF are dispersed in lower volume (50 vol.% of Al). The dense carbon fiber network  
179 observed in Al/vol.%(40GF+10CF) will be used in order to explain further physical properties of the Al/(GF+CF)  
180 composite materials.

181

182 Figure 5 shows an energy dispersive X-ray spectroscopy (EDS) scan realized on (Al+Al-Si)/50vol.%CF composite  
183 material in order to highlight the distribution of the silicon inside the Al matrix. Fig. 5.b shows the microstructure  
184 of Al/CF composites fabricated solid-liquid phase sintering respectively. It shows the presence of white area in the  
185 (Al+Al-Si)/50vol.%CF, more precisely in the Al matrix, Al-CF interface and CF/CF contact points. These white  
186 parts were not observed in composites fabricated by conventional PM route. The spot 1 and 2 correspond to the  
187 aluminum matrix and carbon fiber, respectively. The spots scan 3, 4 and 5 reveals the presence of aluminum and  
188 silicon in the white area, which corresponds to the Al-12wt%Si phase. Then, EDS scan confirms the infiltration of  
189 the liquid phase in the porosity between Al particles, Al-CF interphase and CF/CF contact point during the  
190 sintering process.



191

192

193 Figure 5: EDS spot scan analysis of (Al+Al-Si)/50vol.% CF (a and b) composite material

194

195 3.2. Optimization of solid-liquid phase sintering

196 The amount of Al-12wt%Si were optimized for a GF content of 50 vol.% in order to achieve a fully dense  
 197 composite materials and to show its effect on the in-plane TC. Table 1 shows the evolution of the measured relative  
 198 density of the (Al+Al-Si)/50vol.%GF composite materials with the volume percentage of Al-12w%Si liquid phase  
 199 ranging from 0 to 15 vol.% with 2.5 vol.% step increase. It is well known that the relative density of composites  
 200 decreases when the reinforcement content increases [16, 18]. Indeed, in addition to the porosity, which is inherent  
 201 to the powder metallurgy (PM) route, the decrease of the relative density may be correlated with the Al-GF  
 202 interfacial nano-voids [26] and graphite-graphite contact points (Fig. 3 and 4) which appear significantly from a  
 203 carbon volume fraction close to 30 vol.%GF [10, 18]. Al/50vol.%GF composite fabricated by conventional PM  
 204 route shows a relative density of 97.5%. When the volume percentage of liquid phase increases, the relative density  
 205 increases to reach a value of 98.5% for a liquid content of 15 vol.%. This behavior is explained by the fact that the  
 206 liquid phase formed during the sintering step, reduces the pores and infiltrates the GF/GF contact point where no  
 207 sintering can occurs. Therefore, the liquid phase sintering helps to increase the relative density of Al/C composite  
 208 materials with high carbon content. With this fabrication process, MMC, with carbon volume fraction up to 70%,  
 209 have been successfully fabricated with a porosity level smaller than 3%.

210 Table 1: Influence of the Al-12wt%Si liquid content (vol.%) on the relative density (%) and the in-plane TC  
 211 (W/m.K)

Liquid phase content (vol.%)	0	2.5	5	7.5	10	12.5	15
Relative density (%)	97.5	97.9	98.1	98.3	98.2	98.3	98.5
In-plane TC (W/m.K)	400	404	425	423	428	414	409

212

213 Moreover, Table 1 shows that the evolution of the relative density can be correlated with the evolution of the TC.  
 214 In the in-plane direction, the graphite flakes are oriented parallel to the direction of thermal conduction  
 215 measurement. Al/50vol.%GF composite fabricated by conventional PM route shows an in-plane TC of 400  
 216 W/m.K. From 0 to 5 vol.% of liquid phase, the in-plane TC increases from 400 to 425 W/m.K. Then, from 5 to 10  
 217 vol.% of liquid phase, the in-plane TC reaches values close to 425 W/m.K, and then decreases at 409 W/m.K for  
 218 higher Al-Si content. It has also to be noticed that, whatever the Al-Si content, the in-plane TC of (Al+Al-Si)/GF  
 219 composites are always higher than the Al/50vol.%GF fabricated by conventional PM route. This behavior can be  
 220 explained by two factors: 1) the increase of relative density with the liquid phase content and 2) the lower intrinsic  
 221 TC of Al-12wt%Si alloy compared to the pure Al (experimental values of 163 W/m.K and 217 W/m.K,  
 222 respectively). Indeed, the increase of TC from 0 to 10 vol.% of liquid phase is correlated to the increase of the  
 223 relative density of (Al+Al-Si)/GF composite materials. Then, from 10 to 15 vol.% of Al-Si, even if the relative  
 224 density increases slightly, the important quantity and the intrinsic TC of Al-Si alloy, results in a decrease of the  
 225 in-plane TC of (Al+Al-Si)/50vol.%GF composite materials. Hence, a volume percentage of 10% were selected in  
 226 order to fabricate (Al<sub>90vol.%</sub>+Al-Si<sub>10vol.%</sub>)/50vol.%Carbon composites, where the carbon is a mixture of graphite  
 227 flakes and carbon fibers.

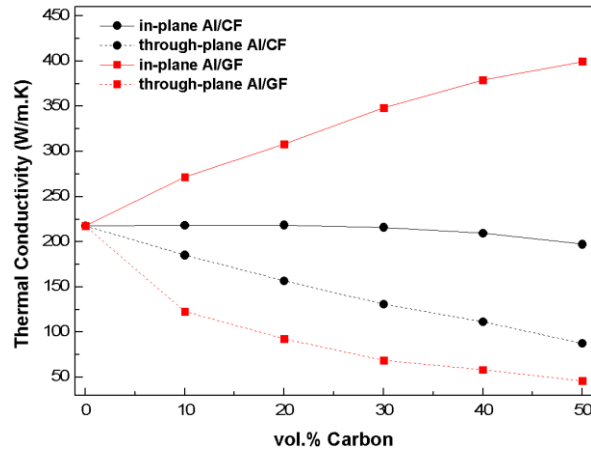
228

### 229 3.3. Thermal conductivity of Al/GF and Al/CF composite materials

230 Al/GF and Al/CF composites were fabricated in order to evaluate the individual effect of the GF and CF on the  
 231 thermal properties of Al/C composite materials. Figure 6 shows the evolution, of the in-plane and through-plane  
 232 TC of Al/GF and Al/CF composites with different carbon volume fraction. First of all, Fig. 6 shows a TC of 218  
 233 W/m.K for the sintered Al powder. (TC of 239 W/m.K is reported for high purity aluminum at 70°C [30]). The  
 234 difference between sintered and high purity aluminum materials (foundry route) is mainly attributed to the residual  
 235 porosity and the amorphous aluminum oxide presents on the surface of each aluminum grain when using PM route.

236 In the in-plane direction, the graphite flakes are preferentially oriented parallel to the direction of thermal  
237 conduction measurement. Then, the TC increases with the graphite content to reach a value of 400 W/m.K. This  
238 behavior is in accordance to the intrinsic in-plane TC of the GF (close to 1000 W/m.K [10-11]). The TC of the  
239 Al/CF composites decreases slightly from 218 to 216 W/m.K from 0 to 30 vol.% of CF and then reach a value of  
240 197 W/m.K from 30 to 50 vol.% of CF. This slight decrease of TC may be explained by the fact that, due to the  
241 random distribution of the CF in the plane of measurement, the supposed intrinsic TC of the CF in the plane, 280  
242 W/m.K [16] is an average of the along (550 W/m.K; manufacturer data) and perpendicular to the CF axis (5-10  
243 W/m.K). Thermal resistance at the Al-C interface and the decrease of the relative density with the increase of  
244 carbon content can explain the slight decrease of in-plane TC of Al/CF composite materials.

245 In the through-plane direction (dotted line), the GF and CF are preferentially oriented perpendicularly to the  
246 direction of thermal conduction measurement. Then, the TC decreases with the carbon content to reach a value of  
247 87 and 46 W/m.K for Al/GF and Al/CF composites, respectively. This decrease is in accordance to the intrinsic  
248 through-plane TC of the GF and CF (5-10 W/m.K [10-11]). However, the behavior of through-plane TC with the  
249 carbon content differs between the two reinforcements. Indeed, in the Al/GF composites, the variation of the TC  
250 with the GF content has a behavior of an inverse function: a drastic decrease of TC from 0 to 10 vol.% of GF (218  
251 to 123 W/m.K: 43% of decrease) and a slower decrease of TC from 10 to 50 vol.% of GF (123 to 46 W/m.K: 62%  
252 of decrease). In contrast, the TC of Al/CF composites decreases linearly with CF content and stay higher than  
253 Al/GF for 50vol.% of carbon. This difference of behavior can be explained by the difference of morphology of the  
254 reinforcement. Indeed, the planar morphology and larger size (average size and thickness of 550  $\mu\text{m}$  and 30  $\mu\text{m}$ ,  
255 respectively) than CF (average length and diameter of 250  $\mu\text{m}$  and 10  $\mu\text{m}$ , respectively) allow the GF to slow the  
256 thermal flow more efficiently than CF in the through-plane direction. Moreover, the orientation of the  
257 reinforcement, in a plane perpendicular to the pressure direction, which is induced by the hot-pressing process, is  
258 easily achieved for the GF than for the CF (Fig. 5a).



259

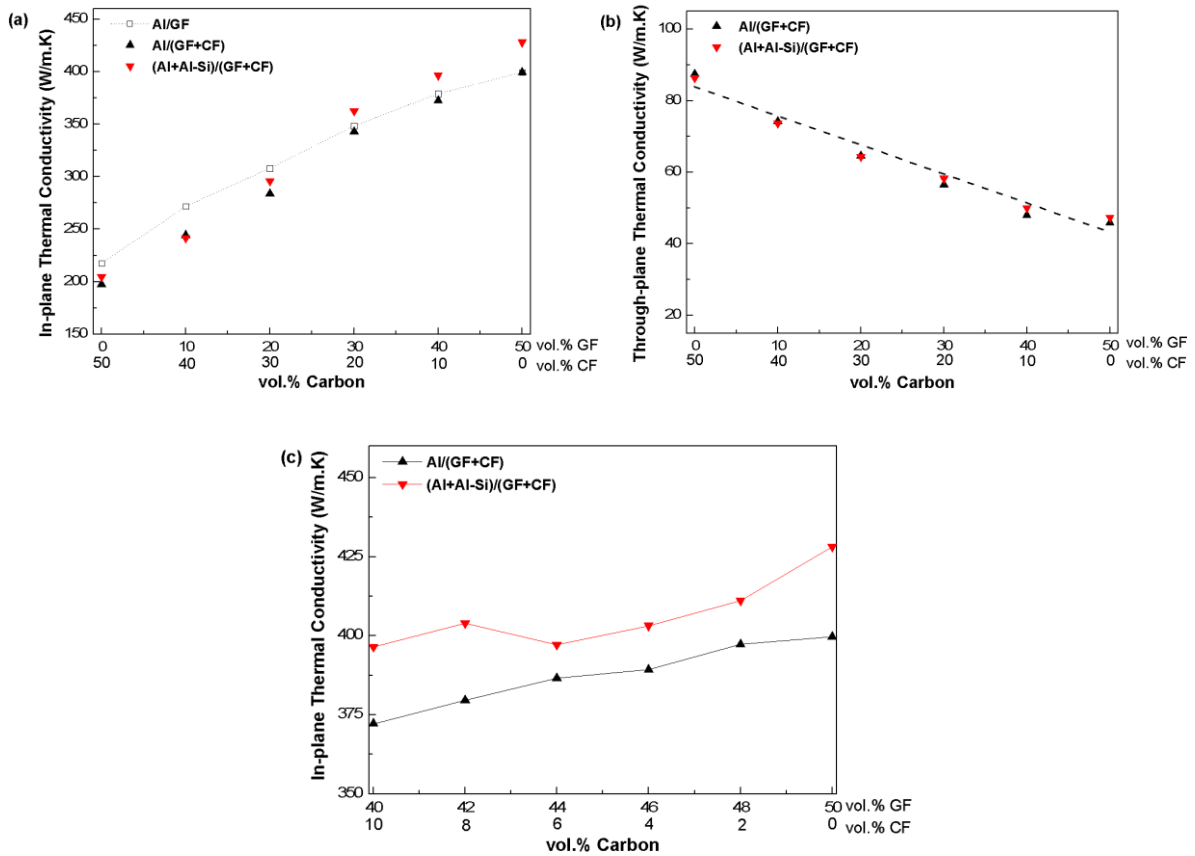
260 Figure 6: Comparison of experimental TC of Al/GF (red square) and Al/CF (black circle) composite materials in  
 261 the through-plane (dotted line) and in-plane (line) direction (standard deviation 5%)

262

### 263 3.4. Thermal conductivity of Al/(GF+CF) and (Al+Al-Si)/(GF+CF) composite materials

264 Figure 7 shows the evolution of the CT of Al/(GF+CF) and (Al<sub>90vol.%</sub>+Al-Si<sub>10vol.%</sub>)/(GF+CF) composites with a  
 265 total carbon content of 50 vol.%, in the in-plane (Fig. 7a and 7c) and through-plane (Fig. 7b) directions. For  
 266 comparison purpose, the CT of Al/GF composite materials was added in Fig. 7a (dotted line). It can be shown that  
 267 the in-plane TC of the Al/(GF+CF) composites is lower than the Al/GF composites with the same volume content  
 268 of GF. It should be noted that the gap between the two sets of materials decreases when the GF/CF ratio increases.  
 269 Indeed, as shown in Fig. 6, the decrease of the in-plane TC of Al/CF is negligible between 0 to 30 vol% of CF  
 270 which explains the weak gap between Al/(GF+CF) and Al/GF from a carbon content of (30 vol.%GF + 20  
 271 vol.%CF). For higher CF content a decrease of the in-plane TC of Al/(GF+CF), compared to Al/GF with the same  
 272 GF content, is observed. Fig. 7b shows the through-plane TC of Al/(GF+CF) composites materials. It can be seen  
 273 an almost linear behavior of the TC of Al/(GF+CF) composite materials.

274 The Al/(GF+CF) composite materials fabricated by conventional PM route (black triangle) were compared to the  
 275 equivalent composites fabricated by solid-liquid phase sintering (red triangle). It can be seen that solid-liquid phase  
 276 sintering provides an increase of the in-plane TC (Fig. 7a and 7c). As explained in section 4.2, the liquid phase  
 277 sintering tends to increase the relative density of Al/C composite materials with high carbon content by infiltrating  
 278 the pores and the carbon-carbon contact points where no sintering can occur.



279

280

281 Figure 7: Experimental CT of  $(Al_{90vol.}+Al-Si_{10vol.})/(GF+CF)$  (red triangle) and  $Al/(GF+CF)$  (black triangle)  
 282 composite materials in (a and c) the in-plane direction and (b) through-plane (b) direction (standard deviation 5%)

283

284 This increase of the relative density of  $Al/50vol. C$  and interfacial chemical reactions provides an enhancement  
 285 of the in-plane TC. Indeed, as it can be seen on Fig. 8, small voids, located at the  $Al-CF(GF)$  interface, can be  
 286 observed on TEM micrographs of  $Al/CF$  (Fig. 8 a) whereas no such of voids are observed on  $(Al+Al-Si)/CF$   
 287 composite materials (Fig. 8 b). Also, the  $Al-Si$  liquid phase can induce the formation of Aluminum carbide ((Fig.  
 288 8 b), at the  $Al-CF$  interface, inducing a better property transfer between the matrix and the reinforcements.

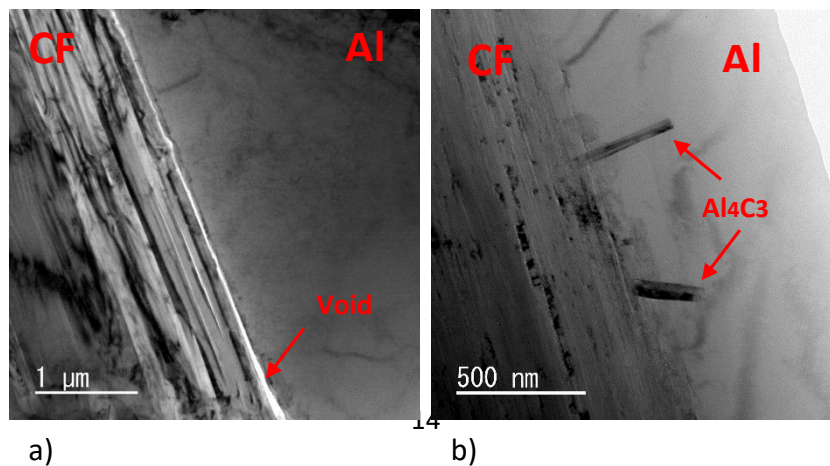
289

290

291

292

293



a)

b)

294 Figure 8: TEM micrographs of a) Al/CF composite material and b) al-Al-Si/CF composite material

295

296 In the through-plane direction, no significant effect of the solid-liquid process is observed which shows that the  
297 through-plane TC were not linked to the relative density like the interfacial thermal resistance, as shown by S. Ren  
298 et al. [26].

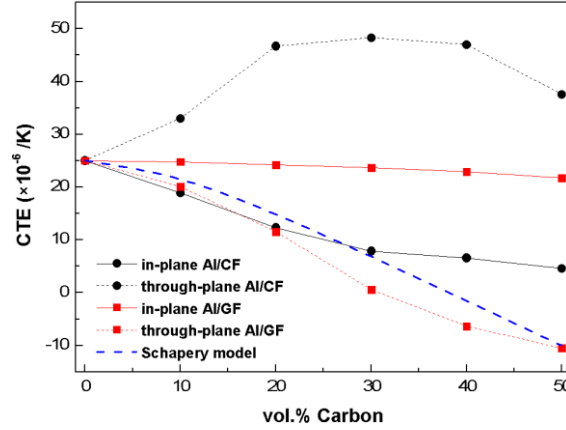
299

### 300 3.5. Thermal expansion of Al/GF and Al/CF composites materials

301 Figure 9 shows the evolution of the CTE of Al/GF and Al/CF composites with different carbon volume fraction,  
302 in the in-plane and through-plane directions. The CTE of pure Al matrix fabricated by PM route has a value of  
303  $25 \times 10^{-6}$  /K. Al/GF and Al/CF composites show different behaviors, for the two directions of measurement.  
304 Concerning Al/CF composites, a decrease of the in-plane CTE is observed and reaches a value of  $4.6 \times 10^{-6}$  /K for  
305 a CF content of 50 vol.%. This result is in accordance with the intrinsic in-plane CTE of CF ( $-1 \times 10^{-6}$  /K). However,  
306 the through-plane CTE of Al/CF composites show an important increase between 0 and 20 vol.% of CF, before to  
307 reach a maximum value of  $47 \times 10^{-6}$  /K from 20 to 40 vol.% and finally, a decrease at 50 vol.% CF. Unlike the  
308 evolution of the in-plane CTE, this behavior is in contradiction with the intrinsic through-plane CTE of CF ( $12-$   
309  $15 \times 10^{-6}$  /K [8]). Considering the fact that the CFs restrain the dilatation of Al in the in-plane direction leads to a  
310 compressive strain in the same direction and then a decrease of the in-plane CTE [31]. This in-plane compressive  
311 strain induces an increase of through-plane CTE because of the positive Poisson ratio of Al and CF (0.345 [25]  
312 and 0.2 [32], respectively).

313 Concerning the Al/GF composites, the CTE differ radically in the two directions of measurement. In the in-plane  
314 direction, the CTE decreases slightly to a value of  $21.8 \times 10^{-6}$  /K for 50 vol.% of GF. In the through-plane direction,  
315 the CTE decreases drastically and reaches a negative value of  $-10.5 \times 10^{-6}$  /K for 50 vol.% of GF. These counter-  
316 intuitive behaviors were reported in several studies for Al/GF and Cu/GF systems [26-29]. In order to understand  
317 these behaviors, Firkowska et al. [27] modeled the mechanical and thermal interplay of graphite and Copper within  
318 elasticity theory and considered a sandwich-like structure of graphite and Copper. They found that the temperature-  
319 dependent in-plane strain in the graphite embedded in a matrix copper results in a negative through-plane CTE  
320 ( $\alpha_{33}$ ) of  $-26 \times 10^{-6}$  /K calculated by equation (1)  $\alpha_{33} = \frac{d\varepsilon_{33}}{dT} = \alpha_{gr,3} + v_{2D} \Delta\alpha_X - \frac{dv_{2D}}{dT} \varepsilon_{11}^0$  where  $\varepsilon_{33}$  and T are the  
321 through-plane strain of the graphite and the temperature, respectively.  $\alpha_{gr,3}$  is the intrinsic through-plane CTE of  
322 graphite ( $28 \times 10^{-6}$  /K).  $v_{2D}$  and  $\frac{dv_{2D}}{dT} = -4.3 \times 10^{-2}$  /K are the 2D equivalent Poisson ratio of graphite and its

323 temperature derivative.  $\varepsilon_{11}^0 \sim -10^{-3}$  is the estimated residual in-plane strain of graphite in Copper matrix.  $\frac{d\varepsilon_{11}}{dT} =$   
 324  $\Delta\alpha_X$  is the temperature derivative of the in-plane strain  $\varepsilon_{11} = \varepsilon_{22}$  in graphite and it is calculated using equation (2)  
 325  $\frac{d\varepsilon_{11}}{dT} = \Delta\alpha_X = \alpha_X - \alpha_{gr,1}$  where  $\alpha_x$  and  $\alpha_{gr,3}$  are the in-plane CTE of Cu/50vol%GF and GF, respectively. The  
 326 equation (1) shows that the change of CTE value (from  $28 \times 10^{-6} /K$  to  $-26 \times 10^{-6} /K$ ) is due to the large Poisson  
 327 ratio of graphite ( $\nu_{2D}$ ) and its strong temperature dependence.



328  
 329 **Figure 9:** Comparison of experimental CTE of Al/GF (red square) and Al/CF (black circle) composite materials in  
 330 the through-plane (dotted line) and in-plane (line) direction. Theoretical predictions by the Schapery model (blue  
 331 dashed line) for Al/GF system in the through-plane direction (standard deviation 3%)

332  
 333 We propose here to use the formulation (1) of Firkowska et al. [27] to explain the behavior of through-plane CTE  
 334 of Al/GF composite materials and explain the important decrease of the CTE compared to Cu/GF system. The in-  
 335 plane lattice constant of the GF follows the CTE of the composites which causes an in-plane strain  $\varepsilon_{11} = \varepsilon_{22}$  in the  
 336 GF that varies with temperature as shown on equation (2). In Al/GF system, an in-plane CTE of  $21.8 \times 10^{-6} /K$  for  
 337 50 vol.% of GF was obtained, which is higher than in plane CTE of Cu/50vol.%GF reported in previous studies  
 338 ( $14 \times 10^{-6} /K$  [26],  $12 \times 10^{-6} /K$  [27] and  $13.6 \times 10^{-6} /K$  [28]). This difference is due to the higher intrinsic CTE of  
 339 Aluminum compared to Copper ( $24 \times 10^{-6} /K$  and  $17 \times 10^{-6} /K$ , respectively [1]). Then the higher in-plane CTE  
 340 difference of Al/GF and GF ( $\alpha_{gr,1} = -1 \times 10^{-6} /K$ ) induce a higher in-plane strain in the GF. For an Al/GF system  $\Delta\alpha_x$   
 341 is equal to  $22.8 \times 10^{-6} /K$  which is higher than Cu/GF system. In a second step, intrinsic strain, induced by the CTE  
 342 difference of the different constituent, has to be consider. Indeed, after the consolidation step, when the temperature  
 343 decreases to room temperature, the reinforcement and the matrix shrink at different rates, which induce a residual  
 344 in-plane strain  $\varepsilon_{11}^0$  equal to  $\sim -10^{-3}$  for Cu/GF system [27]. Considering that  $CTE_{Al}$  is  $\sim 1.5$  higher than  $CTE_{Cu}$ , it can

345 be reasonably assumed that the in-plane residual  $\varepsilon_{11}^0$  of Al/GF system is also 1.5 times higher than  $\varepsilon_{11}^0$  for Cu/GF  
 346 system. By using the formulation (1), a value of  $-54 \times 10^{-6}/\text{K}$  was calculated for the through-plane CTE of GF which  
 347 is quite different from the intrinsic CTE value of the through-plane GF ( $28 \times 10^{-6}/\text{K}$ ). This calculated value will be  
 348 used to calculate theoretical values of CTE for the Al/GF composite materials.

349 Schapery model [32] was chosen to predict the CTE of the Al/GF system with anisotropic properties [33] and then  
 350 compared with the obtained experimental values:

$$351 \quad \alpha_{c,2} = V_m(1 + v_m)\alpha_m + V_f(1 + v_{f,2})\alpha_{f,2} - \alpha_{c,1}v_{c,1} \quad (3)$$

$$352 \quad \text{With } \alpha_{c,1} = \frac{V_f\alpha_{f,1}E_{f,1} + V_m\alpha_m E_m}{V_f E_{f,1} + V_m E_m} \quad (4) \quad \text{and} \quad v_{c,1} = V_m v_m + V_f v_{f,1} \quad (5)$$

353 In these equations,  $\alpha$ ,  $V$ ,  $E$  and  $v$  are the CTE, the volume fraction, the Young's modulus and the Poisson's ratio,  
 354 respectively. 1 and 2 refer to in-plane and through-plane direction, respectively. The subscripts c, m, and f refer to  
 355 composite, matrix and reinforcement, respectively. The material parameters for the calculations are given in Table  
 356 2 and the through-plane CTE of GF used in this model is the value calculated with the Firkowska formulation [27].

357 Table 2: Materials parameters for calculating the theoretical CTE for Al/GF composite materials

Material	$\alpha$ ( $10^{-6}/\text{K}$ )	E (GPa)	$v$	Ref.
In-plane GF	-1	1109	0.12	[34]
Through-plane GF	-58*	38.7	0.01	[27]*; [34]
Al	25	69	0.345	[25]

358 \*Value calculated with Firkowska formulation [27]

359 Figure 8 shows a comparison of the theoretical values of the through-plane CTE of Al/GF composite materials  
 360 (blue dashed line), calculated using Schapery model (3) and Firkowska formulation (1) with the experimental  
 361 values for fabricated Al/GF composites materials. The Schapery prediction is in fairly good agreement with the  
 362 experimental CTE of Al/GF composite materials in the through-plane direction. We can therefore argue that the  
 363 Firkowska formulation, given for Cu based materials, can be transposed for an Al/GF system and allows to  
 364 demonstrate that the higher mismatch between the matrix and the GF for a Al/GF system compared to a Cu/GF  
 365 system, induce a higher in-plane strain on the GF and resulting in a through-plane CTE for Al/GF composites  
 366 significantly lower than for Cu/GF composites.

367

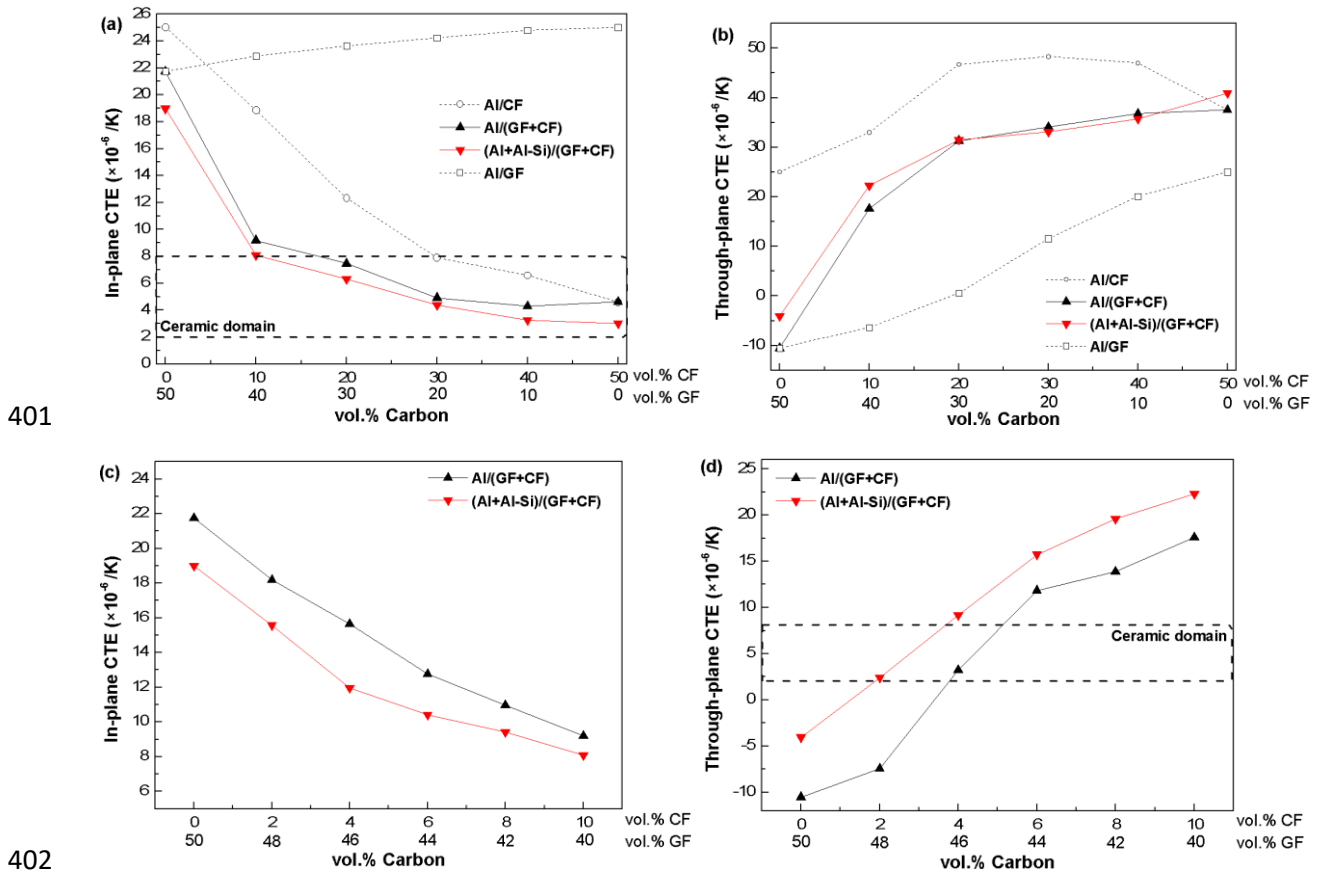
### 368 3.6. Thermal expansion of Al/(GF+CF) and (Al+Al-Si)/(GF+CF) composite materials

369 Figure 10 shows the evolution of the CTE of Al/(GF+CF) and (Al<sub>90vol.%</sub>+Al-Si<sub>10vol.%</sub>)/(GF+CF) composites with a  
370 total carbon volume percentage of 50%, in the in-plane (Fig. 10a and c) and through-plane (Fig. 10b and c)  
371 directions. For comparison purpose, the CTE of Al/CF and Al/GF composites were added to this figure (dotted  
372 line). For pure GF reinforcement, in the in-plane direction, the CTE of the composites decreases slightly to reach  
373 value of  $21.8 \times 10^{-6} /K$  for 50 vol.% of GF. However, with a mix carbon composition (CF + GF), a huge decrease  
374 for a CF vol. % up to 10% ( $9 \times 10^{-6} /K$ ) is observed (a detail of this variation is given in Fig. 10c) follow by a slower  
375 decrease to reach the CTE value of the Al/50vol.%CF material ( $4.6 \times 10^{-6} /K$ ).

376 Considering that GF alone has no significant effect on the in-plane CTE, Al/(40vol.%GF + 10vol.%CF) can be  
377 compared to Al/10vol.%CF composite material. It can be show that for the same content of CF, the CTE decreases  
378 from  $18.9 \times 10^{-6} /K$  to  $9.2 \times 10^{-6} /K$ . Favier et al. [35] reported that the geometric percolation of cylindrical  
379 reinforcement, with an aspect ratio of 25, is close to 3 vol.% and 18 vol.% for a 3D and 2D random orientation,  
380 respectively. However, the geometric percolation should be distinguished from the mechanical percolation. Indeed,  
381 for electrical system, the geometric percolation is identical with the electric percolation. However, for thermo-  
382 mechanical properties, the geometric percolation is not enough to ensure the rigidity of the whole system. Then,  
383 the mechanical percolation, which is higher than the geometric percolation, should be considered. The mechanical  
384 percolation of the CF in Al/CF composite materials have already been associated to the formation of rigid skeleton  
385 of reinforcement, from a CF volume fraction close to 30 vol.% [8]. This behavior may explain the slope change of  
386 the in-plane CTE observed from 30 vol.% of CF (Fig. 10a). The addition of graphite to the CF provides the  
387 formation of rigid CF skeleton with only 10 vol.% of CF. Indeed, as it was demonstrated by X-Ray tomography,  
388 the CF network in Al/10vol.% is not enough dense to build a rigid skeleton, and thus the mechanical percolation  
389 is not reached. The huge decrease of CTE for the CF + GF reinforcement can therefore be attributed to the  
390 formation of a rigid CF skeleton in-between the network of the graphite flakes. Moreover, the fact that CF are  
391 interleaved between GF may prevent the disorientation of CF out of (xy) plane, as observed in Al/10vol.%CF  
392 composite material (Fig. 4h).

393 In the through-plane direction, the CTE increases significantly from a value of  $-10.5 \times 10^{-6} /K$  for 50 vol.% of GF  
394 to a value of  $37.6 \times 10^{-6} /K$ . Indeed, for a carbon composition of (40 vol.%GF + 10 vol.%CF), an important increase  
395 of the CTE is observed and reach a value of  $17.6 \times 10^{-6} /K$  (a detail of this variation is given in Fig. 9d). Then, when  
396 the CF/GF ratio increases, the CTE increases slowly to tend to the CTE of Al/50vol%CF ( $37.8 \times 10^{-6} /K$ ). Therefore,  
397 the addition of CF to the GF provides an important CTE increase of Al/(GF+CF) composite material due to the

398 individual effect of the CF in the through-plane direction showed in Fig. 10b (circle mark and dotted line). The  
 399 fact that the through-plane CTE decreases in Al/GF composites and increases in Al/CF composites explains the  
 400 behavior of Al/(GF+CF) composites materials.



403 Figure 10: Experimental CTE of  $(Al_{90vol.\%}+Al-Si_{10vol.\%})/(GF+CF)$  (red triangle) and  $Al/(GF+CF)$  (black triangle)  
 404 composite materials in (a and c) the in-plane direction and (b and c) the through-plane direction (standard deviation  
 405 5%)

406

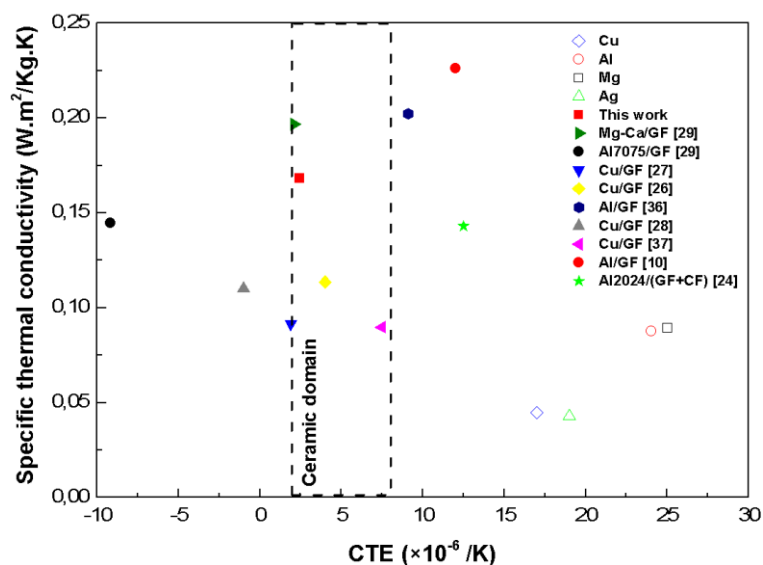
407 Figure 10 also shows the CTE behavior of the Al based composite materials fabricated using solid-liquid phase  
 408 sintering (red triangle) where Al-Si eutectic alloy is added to Al. It can be shown that solid-liquid phase sintering  
 409 provides a decrease of the in-plane CTE and an increase of the through-plane CTE of  $(Al_{90vol.\%}+Al-$   
 410  $Si_{10vol.\%})/(GF+CF)$  in comparison to the  $Al/(GF+CF)$  composite materials. As shown earlier, the Al-Si liquid phase  
 411 was observed between the Al particles, at the Al/C interface and at the carbon-carbon contact points (Fig. 5). The  
 412 presence of the Al-Si liquid phase at the C-C contact points allows soldering the carbon reinforcement in this zone  
 413 and therefore to consolidate the carbon rigid network observed by x-ray tomography (Fig. 4). The formation of

414 this carbon rigid network, induced by the liquid phase, can explain the decrease of the in-plane CTE of Al/(GF+CF)  
 415 composite materials. The fact that the solid-liquid phase sintering generates a decrease of the in-plane CTE and an  
 416 increase of the through-plane CTE (in average), compared to the PM route shows that the physical properties of  
 417 the Al based composites in two direction are linked. This behavior is in accordance with the Firkowska formulation  
 418 (eq. 1). Indeed, the reduction of the in-plane CTE of Al/50%vol.GF composites with the solid-liquid phase  
 419 sintering (from  $21.8 \times 10^{-6} /K$  to  $19 \times 10^{-6} /K$ ) induces a decrease of  $\Delta\alpha_x$  (eq. 2) and in-plane strain  $\varepsilon_{11} = \varepsilon_{22}$ . Then, the  
 420 through-plane CTE of GF embedded in the matrix ( $\alpha_{33}$  eq. (1)) will increase. This explains, therefore, the increase  
 421 of the through-plane CTE of Al/GF composites with the solid-liquid phase sintering (from  $-10.5 \times 10^{-6} /K$  to -  
 422  $4.1 \times 10^{-6} /K$ ). With the addition of small amount of CF, the CTE value of (Al+Al-Si)/C composite fabricated by  
 423 solid-liquid phase sintering can be controlled in order to obtain a CTE compatible to the ceramic domain ( $2 \times 10^{-6}$   
 424  $/K$  to  $8 \times 10^{-6} /K$ ) in the in-plane direction or through-plane direction (Fig. 9a and 9d) without affecting significantly  
 425 the in-plane TC of the composite materials (Fig. 7c).

426

### 427 3.7. Specific thermal conductivity of Al/(GF+CF) composite materials

428 Figure 11 shows the specific TC of Metal/C (with a reinforcement content close to 50 vol.%) composites materials  
 429 in function of CTE reported in the literature. Thanks to the low density of Al/50vol.%C ( $2.44 \text{ g/cm}^3$ ) and a high  
 430 TC ( $411 \text{ W/m.K}$ ), our MMC shows a high specific TC even higher than Cu/GF composite materials. Moreover  
 431 Al/(GF+CF) shows a low CTE which make these composite materials compatible with electronic applications. In  
 432 the ceramic domain, only Mg-Ca/GF composite shows a higher specific TC than our work thanks to the lightweight  
 433 of the matrix.



434

435 Figure 11: Specific TC of (Al<sub>90vol.%</sub>+Al-Si<sub>10vol.%</sub>)/(GF+CF) (red square) compared to the Metal/C composite  
436 materials reported in the literature

437

#### 438 4. Conclusion

439 The addition of 50 vol.% of GF into the Al matrix improves remarkably the in-plane TC (400 W/m.K). However,  
440 these materials show a through-plane CTE ( $-10.5 \times 10^{-6}$  /K) and in-plane CTE ( $21.8 \times 10^{-6}$  /K) incompatible with  
441 ceramic domain. Carbon fibers were added to Al/GF composite in order to increase the through-plane CTE and to  
442 decrease the in-plane CTE of Al/GF composites materials. It has been shown that by addition of  
443 (40vol.%GF+10vol.%CF) to the Al matrix, induces a decrease of the in-plane CTE to  $9.2 \times 10^{-6}$  /K which is  
444 significantly lower than an Al/10vol.%CF and Al/40vol.%GF composite materials ( $18.9 \times 10^{-6}$  /K and  $22.9 \times 10^{-6}$   
445 /K, respectively). The GF, in addition to increase the TC of the matrix, allows to decrease the mechanical  
446 percolation threshold of carbon fibers and then, provide the formation of a continuous and rigid (GF+CF) network  
447 that enhance the decrease of in-plane CTE.

448 In the through-plane direction, it has been shown that Al/(40vol.%GF+10vol.%CF) composite exhibits a CTE of  
449  $17.6 \times 10^{-6}$  /K which is significantly higher than an Al/40%GF ( $-6.4 \times 10^{-6}$  /K) composite and lower than  
450 Al/10vol.%CF ( $33 \times 10^{-6}$  /K) composite. Recognizing that CF allows to increase the through-plane CTE, the GF/CF  
451 ratio was optimized for a total reinforcement of 50 vol% in order to control the value of the CTE without decrease  
452 significantly the in-plane TC of the composite materials.

453 Solid-liquid phase sintering was used to fabricate Al/C composites. The amount of liquid phase alloy was  
454 optimized for a carbon content of 50 vol.%. The addition of 10 vol.% of Al-12wt%Si alloy to the matrix of Al/C  
455 composite materials induces:

- 456 • The increase of the relative densification of composite materials for reinforcement content of 50 vol.%.
- 457 • The increase of the in-plane TC of Al/GF composite from 400 to 428 W/m.K.
- 458 • The decrease of the in-plane CTE and the increase of through-plane CTE of Al/C composites materials.
- 459 • The presence of liquid phase in the carbon-carbon contact points leads to the formation of a solid CF+GF  
460 network.

461 Finally, two sets of (Al<sub>90vol.%</sub>+Al-Si<sub>10vol.%</sub>)/50%Carbone composite materials have been developed and optimized:

- 462 • High in-plane TC (363 W/m.K) and low in-plane CTE ( $6.3 \times 10^{-6}$  /K)

463           • High in-plane TC (411 W/m.K) and low through-plane CTE ( $2.4 \times 10^{-6}$  /K)

464 Therefore, with their remarkable specific TC ( $0.168 \text{ W.m}^2/\text{Kg.K}$ ), the composite materials developed in this study  
465 are applicable as a lightweight heat sink in microelectronic industries.

466

467 Acknowledgement

468 The authors thank the University of Bordeaux (2015-FD-24) for financial support.

469 References

470 [1] C. Zweben, JOM, 50 (6), 47-51b(1998)

471 [2] C. Zweben: Annual IEEE Semiconductor Thermal Measurement and Management Symposium, 168-174  
472 (2005)

473 [3] E. Rohatgi, K. Pradeep, Defence Science Journal, 43 (4), 323-349 (1993)

474 [4] S. Mallik, N. Ekere, C. Best, R. Bhatti, R, Applied Thermal Engineering, 31 (2-3), 355-362 (2011)

475 [5] K. Yoshida, H. Morigami, Microelectronics Reliability, 44 (2), 303-308 (2004)

476 [6] P.W. Ruch, O. Beffort, S. Kleiner, L. Weber, P.J. Uggowitzner, Composites Science and Technology, 66 (15),  
477 2677-2685 (2006)

478 [7] O. Beffort, F.A. Khalid, L. Weber, P. U.E. Ruch, Klotz, S. Meier, S. Kleiner, Diamond and Related Materials,  
479 15 (9), 1250-1260 (2006)

480 [8] H. Kurita, E. Feuillet, T. Guillemet, J.-M. Heintz, A. Kawasaki, J.-F. Silvain, Acta Metallurgica Sinica (English  
481 Letters), 27 (4), 714-722 (2014)

482 [9] H.O. Pierson, Handbook of Carbon, Graphite, Diamond and Fullerenes, Noyes Publications Park Ridge (New  
483 Jersey, USA), 194-195 (1993)

484 [10] J.K. Chen, I.S. Huang, Composites Part B: Engineering, 44 (1), 698-703 (2013)

485 [11] M. Murakami, N. Nishiki, K. Nakamura, J. Ehara, H. Okada, T. Kouzaki, K. Watanabe, S. Yoshimura,  
486 Carbon, 30 (2), 255-262 (1992)

487 [12] P.G. Klemens, D.F. Pedraza, Carbon, 32 (4), 735-741 (1994)

- 488 [13] Q. Fu, J. Yang, Y. Chen, D. Li, D. Xu, *Applied Physics Letters*, 106 (3), art. no. 031905 (2015)
- 489 [14] Y. Huang, Y. Su, S. Li, Q. Ouyang, G. Zhang, L. Zhang, D. Zhang, *Composites Part B: Engineering*, Volume  
490 107, 43-50 (2016)
- 491 [15] L. Weber, R. Tavangar, *Scripta Materialia*, 57 (11), 988-991 (2007)
- 492 [16] C. Azina, J. Roger, A. Joulain, V. Mauchamp, B. Mortaigne, Y.F. Lu, J.-F. Silvain, *Journal of Alloys and*  
493 *Compounds*, 738, 292-300 (2018)
- 494 [16] J.M. Molina, E. Louis, *Materials Characterization*, 109, 107-115 (2015)
- 495 [17] N. Chamroune, D. Mereib, F. Delange, N. Caillault, Y. Lu, J.-L. Grosseau-Poussard, J.-F. Silvain, *Journal of*  
496 *Materials Science*, 53(11), 8180-8192 (2018)
- 497 [16] C. Zhou, W. Huang, Z. Chen, G. Ji, M.L. Wang, D. Chen, H.W. Wang, *Composites Part B: Engineering*, 70,  
498 256-2 (2015)
- 499 [17] W. Li, Y. Liu, G. Wu, *Carbon*, 95, 545-551 (2015)
- 500 [18] R. Prieto, J.M. Molina, J. Narciso, E. Louis, *Composites Part A: Applied Science and Manufacturing*, 42 (12),  
501 1970-1977 (2011)
- 502 [19] K. Mizuuchi, K. Inoue, Y. Agari, Y. Morisada, M. Sugioka, M. Tanaka, T. Takeuchi, Y. Makino, *Composites*  
503 *Part B: Engineering*, 42 (4), 825-831 (2011)
- 504 [20] R. Prieto, J.M. Molina, J. Narciso, E. Louis, *Scripta Materialia*, 59 (1), 11-14 (2008)
- 505 [21] V. Oddone, J. Segl, M. Prakasam, M.T. Hartmann, J.-F. Silvain, C. Edtmaier, S. Reich, *Journal of Materials*  
506 *Science*, 53(15), 10910-10919 (2018)
- 507 [22] H. Kurita, T. Miyazaki, A. Kawasaki, Y.F. Lu, J.-F. Silvain, *Composites Part A: Applied Science and*  
508 *Manufacturing*, 73, 125-131 (2015)
- 509 [23] S. Ren, J. Chen, X. He, X. Qu, *Carbon*, 127, 412-423 (2018)
- 510 [24] I. Firkowska, A. Boden, B. Boerner, S. Reich, *Nano Letters*, 15 (7), 4745-4751 (2015)
- 511 [25] J. Chen, S. Ren, X. He, X. Qu, *Carbon*, 121, 25-34 (2017)
- 512 [26] V. Oddone, B. Boerner, S. Reich, *Science and Technology of Advanced Materials*, 18 (1), 180-186 (2017)

- 513 [27] C.Y. Ho, R.W. Powell, P.E. Liley, *Journal of Physical and Chemical Reference Data*, 1 (2), pp. 279-421  
514 (1972)
- 515 [28] V. Oddone, S. Reich, *Physica Status Solidi - Rapid Research Letters*, 11 (6), art. no. e201700090 (2017)
- 516 [29] R.A. Schapery, *Journal of Composite Materials*, 2 (3), 380-404 (1968)
- 517 [30] G. Korb, J. Korab, G. Groboth, *Composites Part A: Applied Science and Manufacturing*, 29 (12), 1563-1567  
518 (1998)
- 519 [31] A. Bosak, M. Krisch, M. Mohr, J. Maultzsch, C. Thomsen, *Physical Review B*, 75 (15), 153-408 (2007)
- 520 [32] V. Favier, R. Dendievel, G. Canova, J.Y. Cavaille, P. Gilormini, *Acta Materialia*, 45 (4), 1557-1565 (1997)
- 521 [33] C. Zhou, G. Ji, Z. Chen, M. Wang, A. Addad, D. Schryvers, H. Wang, *Materials and Design*, 63, 719-728  
522 (2014)
- 523 [34] Q. Liu, X.-B. He, S.B. Ren, C. Zhang, L. Ting-Ting, X.H. Qu, *Journal of Alloys and Compounds*, 587, 255-  
524 259 (2014)
- 525

526 Figure captions

527 Figure 1: SEM micrographs of starting materials: (a) Al powder, (b) Al-Si powder, (c) Graphite flakes (d) Carbon  
528 fibers

529

530 Figure 2: Illustration of the solid-liquid phase sintering process. The initial powder mixture (Al+Al-Si+C) is  
531 sintered under 60 MPa at 600°C which result in the fusion of the Al-12wt%Si alloy

532

533 Figure 3: SEM micrographs (in-plane view) of (a) Al/50vol%GF, (b) Al/(40vol.%GF+10vol.%CF) and (c)  
534 Al/50vol%CF composite materials

535

536 Figure 4: X-Ray tomography analysis of (a, b, c and c) Al/50vol.%GF, (d, e, f, and j) and  
537 Al/(40vol.%GF+10vol.%CF), (g, h, i and k) Al/10vol.%CF composite materials. (Yellow arrows show the  
538 pressure direction)

539

540 Figure 5: EDS spot scan analysis of (Al+Al-Si)/50vol.%CF (a and b) composite material.

541

542 Figure 6: Comparison of experimental TC of Al/GF (red square) and Al/CF (black circle) composite materials in  
543 the through-plane (dotted line) and in-plane (line) direction

544

545 Figure 7: Experimental CT of (Al<sub>90vol.%</sub>+Al-Si<sub>10vol.%</sub>)/(GF+CF) (red triangle) and Al/(GF+CF) (black triangle)  
546 composite materials in the in-plane (a and c) and through-plane (b) direction

547

548 Figure 8: TEM micrographs of a) Al/CF composite material and b) al-Al-Si/CF composite material

549

550 Figure 9: Comparison of experimental CTE of Al/GF (red square) and Al/CF (black circle) composite materials in  
551 the through-plane (dotted line) and in-plane (line) direction. Theoretical predictions by the Schapery model (blue  
552 dashed line) for Al/GF system in the through-plane direction

553

554 Figure 10: Experimental CTE of  $(Al_{90vol.\%}+Al-Si_{10vol.\%})/(GF+CF)$  (red triangle) and  $Al/(GF+CF)$  (black triangle)  
555 composite materials in the in-plane (a and c) and through-plane (b and c) direction

556

557 Figure 11: Specific TC of  $(Al_{90vol.\%}+Al-Si_{10vol.\%})/(GF+CF)$  (red square) compared to the Metal/C composite  
558 materials reported in the literature

559

560 Table 1: Influence of the Al-12wt%Si liquid content (vol.%) on the relative density (%) and the in-plane TC  
561 (W/m.K)

562

Liquid phase content (vol.%)	0	2.5	5	7.5	10	12.5	15
Relative density (%)	97.5	97.9	98.1	98.3	98.2	98.3	98.5
In-plane TC (W/m.K)	400	404	425	423	428	414	409

563

564

565 Table 2: Materials parameters for calculating the theoretical CTE for Al/GF composite materials

Material	$\alpha$ ( $10^{-6}$ /K)	E (GPa)	$\nu$	Ref.
In-plane GF	-1	1109	0.12	[34]
Through-plane GF	-58*	38.7	0.01	[27]*; [34]
Al	25	69	0.345	[25]

566 \*Value calculated with Firkowska formulation [27]

567